



# The fine-scale structure of the quiet solar chromosphere

G. Tsiropoula and K. Tziotziou

National Observatory of Athens, Institute for Space Applications and Remote Sensing,  
15236 Palea Penteli, Greece  
e-mail: georgia@space.noa.gr, e-mail: kostas@space.noa.gr

**Abstract.** We present methods for estimating different physical properties of dark mottles from observations obtained with the MSDP spectrograph mounted on the 50 cm refractor of the Pic du Midi Observatory and on THEMIS (Tenerife). We also present studies of their dynamical evolution and estimates of the role they play in the mass balance and heating of the solar atmosphere.

**Key words.** Sun: chromosphere – Sun: fine structure – Sun: coronal heating

## 1. Introduction

The solar chromosphere, when seen in strong lines, such as Ca II H and K and H $\alpha$ , is highly inhomogeneous. In quiet regions, the principal inhomogeneities are related to roughly cellular patterns, which constitute the “network”. The chromospheric network boundaries are outlined by several elongated bright and dark structures called mottles. Mottles seem to be very important jet-like features. They are considered as the disk counterparts of spicules and also as the principal channels through which mass and energy is supplied from the lower layers of the solar atmosphere to the corona and the solar wind. They have widths in the range of 500-2000 km, heights in the range of 5000-10000 km above the photosphere, lifetimes of 5-10 min and temperatures of the order of 7000-15000 K.

---

*Send offprint requests to:* G. Tsiropoula,  
e-mail: georgia@space.noa.gr

A variety of mechanisms for generating mottles and spicules have been proposed. Tsiropoula et al. (1994) and Tziotziou et al. (2003) provided observational evidence of bi-directional flows in mottles followed by downflows and claimed that this flow pattern is consistent with the one expected to occur in the process of magnetic reconnection. Wilhelm (2000) reported also observations of bi-directional flows along spicules observed at the EUV and proposed magnetic reconnection as the driving mechanism of these structures.

The aim of this work is to present methods for estimating different physical properties of dark mottles, studies of their dynamical evolution and estimates of the role they play in the mass balance and heating of the solar atmosphere.

## 2. Observations

We have used two different sets of observations. The first one was obtained on June

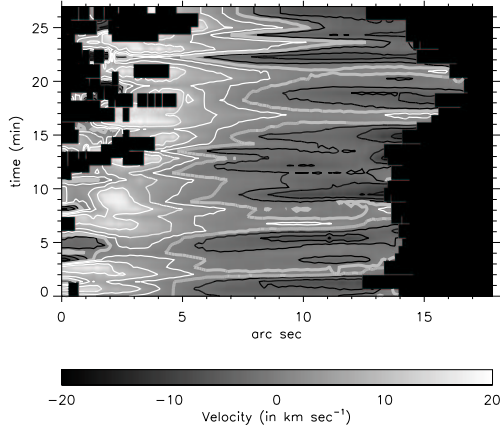


**Fig. 1.** Time slice images of the cloud velocity  $v$  for a cut through an individual mottle observed on May 14, 2000. Black contours denote upward velocities, white contours downward velocities while the thick gray line represents the zero velocity contour.

17, 1986 with the Multichannel Subtractive Double Pass (MSDP) spectrograph installed at the 50 cm refractor of the Pic du Midi Observatory. The second set was obtained on May 14, 2000 with the MSDP spectrograph mounted on the French-Italian solar telescope THEMIS in Tenerife, Canary Islands. The MSDP spectrograph (Mein, 1991, 2002) is designed to record a 2D field-of-view (FOV) at several wavelengths within the line profile. Thus at each pixel of the image the line profile can be reconstructed. A large region of the solar surface can be quickly covered in several wavelengths by displacing the entrance field stop of the telescope. Both time sequences of observations were obtained in the  $H\alpha$  line. Using the MSDP reduction package, intensity and Doppler velocity images at different wavelengths within the  $H\alpha$  line have been obtained.

### 3. Method of computation

For the deduction of different physical parameters of chromospheric structures from observations in the  $H\alpha$  line a method is used which is based in the so called “cloud”

model, introduced by Beckers (1964), (see also Allissandrakis et al., 1990). The model is valid for optically thin structures located well above the background. It considers for an observed intensity profile  $I(\Delta\lambda)$  the contrast profile:

$$\begin{aligned} C(\Delta\lambda) &= \frac{I(\Delta\lambda) - I_0(\Delta\lambda)}{I_0(\Delta\lambda)} \\ &= \left( \frac{S}{I_0(\Delta\lambda)} - 1 \right) (1 - e^{-\tau(\Delta\lambda)}) \end{aligned} \quad (1)$$

with a Gaussian wavelength dependence for the optical thickness:

$$\tau(\Delta\lambda) = \tau_0 e^{-\left(\frac{\Delta\lambda - \Delta\lambda_1}{\Delta\lambda_D}\right)^2} \quad (2)$$

where  $I_0(\Delta\lambda)$  is the reference profile emitted by the background and  $\Delta\lambda_1 = \lambda_0 v/c$  is the Doppler shift with  $\lambda_0$  being the line center wavelength and  $c$  the speed of light. The four adjustable parameters of the model are the source function  $S$ , the Doppler width  $\Delta\lambda_D$ , the optical depth  $\tau_0$  and the line-of-sight (LOS) velocity  $v$ . All these parameters are assumed to be constant through the structure.

## 4. Results

### 4.1. Temporal evolution of the velocity along individual mottles

In Fig. 1 we present the distribution of the velocity as a function of time (time slice image) along the central axis of an individual mottle observed on May 14, 2000. Such time slice images were obtained for several individual mottles and for both data sets (see Tsiropoula et al., 1994; Tziotziou et al., 2003).

On the velocity time slice images we have overplotted some contours of downward (positive) and upward (negative) velocities, as well as the contour of zero velocity. On the velocity images it is clearly seen that the material is almost always descending near the footpoints of the mottles. Higher up there are moments when all (or mostly all) of the material is moving downwards towards the footpoints of the structures. As time progresses, the velocity behaviour usually changes to one where material

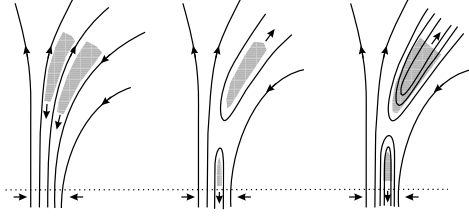


**Fig. 2.** A simple reconnection model (see text) explaining the observed velocity behaviour in mottles.

in the lower part of the mottles is falling down towards the feet of the structures while the material in the upper part is moving upwards. This figure clearly indicates a bi-directional behaviour of the velocity as a function of time with downflows at their footpoints and upflows at their tops. This bi-directional flow is followed by downflowing material along the whole structure and the whole process is repeated with a period of  $\sim 5$  minutes.

The observed velocity behaviour could be explained in the context of a simple reconnection model. A schematic representation of this model is given in Fig. 2. According to this model, the squeezing of opposite polarity field lines at the chromospheric level leads to cooling by radiation of the compressed gas, which is trapped between them and consequently to a downflow due to gravity (left part of Fig. 2). When opposite field lines come too close and reconnection occurs then part of the material is carried upward by the reconnected field lines, while the material below the reconnection region moves downwards under the action of both gravity and magnetic forces (middle and right part of Fig. 2). This cycle is repeated until the field is annihilated.

#### 4.2. Determination of physical parameters

Once the four parameters are determined from the cloud model, the estimation of several other parameters can be made. From the calculated Doppler width values and if we assume a value for the microturbulent velocity,  $\xi_t$ , we can de-

duce the temperature,  $T_e$ . From the optical depth at line center, which may be written as:

$$\tau_0 = \frac{\pi^{1/2} e^2 f \lambda^2 N_2}{m_e c \Delta \lambda_D} d \quad (3)$$

and  $\Delta \lambda_D$ ,  $N_2$ , e.g. the number density in the second hydrogen level, can be obtained. Then the electron density,  $N_e$ , the total particle density of hydrogen (i.e., neutral plus ionized),  $N_H$ , the gas pressure,  $p$ , the total column mass,  $m$ , the mass density,  $\rho$ , can be determined from the following relations:

$$N_e = 3.2 \cdot 10^8 \sqrt{N_2} \text{ cm}^{-3} \quad (4)$$

$$N_H = 5 \cdot 10^8 \cdot 10^{0.5 \log N_2} \quad (5)$$

$$p = k(N_e + 1.0851 N_H) T_e \quad (6)$$

$$m = (N_H m_H + 0.0851 N_H \times 3.97 m_H) d \quad (7)$$

$$\rho = \frac{m}{d} \quad (8)$$

where  $d$  is the path length along the LOS (for details about the derivation of these parameters Tsiropoula & Schmieder (1997)).

#### 4.3. The role of mottles in the mass balance and heating of the solar atmosphere

##### 4.3.1. Mass balance

The parameters obtained in 3 and 4.2 can be used for evaluating the role of mottles in the mass (and in the energy, see 4.3.2) balance of the solar atmosphere. We also remind that mottles arise at the network boundaries attaining maximum upward or downward velocity amplitudes  $v$  of the order of  $25 \text{ km s}^{-1}$  and tend to occur several times at the same location with a typical duration of  $\sim 5$  min.

The upward mass flux of mottles depends on: a) the fraction  $f$  of the solar disk covered by these structures at any given moment, b) the mass density  $\rho$ , and c) the axial upward mottle velocity  $v$ . Taking the total number of mottles on the solar surface to be equal to  $4 \cdot 10^5$  the fraction of the solar surface they cover is

$\sim 0.05$ . As at any given moment only half of the mottles are showing upward motion and from them only half of the material is flowing upwards (assuming that the reconnection occurs in the middle of the structures) the globally averaged mass flux carried upwards can be obtained from the relation:

$$F_M = \frac{1}{2} \left( \frac{1}{2} f \rho v \right) \quad (9)$$

and is equal to  $7.1 \cdot 10^{-9} \text{ g cm}^{-2} \text{ s}^{-1}$ . This value is two orders of magnitude larger than the outward flow of mass from the corona due to the solar wind which is equal to  $3 \cdot 10^{-11} \text{ g cm}^{-2} \text{ s}^{-1}$  (Ulmschneider, 1971). We can conclude from the above estimate that less than 1% of the material of mottles escapes and provides the means by which coronal mass losses in the solar wind is established by material ejected from below. The remainder material returning back to the chromosphere could explain the widespread downflows observed in several EUV lines at the network boundaries.

#### 4.3.2. Energy budget

Magnetic reconnection is considered to be an efficient means of converting magnetic energy into kinetic and thermal energy. We will try to give below a description of the energetics taking into account the different energy components (for more details see Tsiropoula & Tziotziou (2004)). We assume that the energy produced by magnetic dissipation at the reconnection site goes into thermal energy, kinetic energy of the bulk flow, gravitational energy, wave energy, as well as conduction and radiation losses. Our aim is to obtain order of magnitude estimates of the different processes that contribute to the energy budget and to derive an estimate of the energy released. We assume that the reconnection point is located in the middle of the structure. We also consider that the part of the structure below the reconnection point is pulled down and thus the energy provided by the dissipation of the magnetic energy goes to the heating of the chromosphere, while that dissipated above the reconnection point goes to the heating of the corona. Thus we can separate the energy fluxes into those travelling

towards and those travelling away from the observer according to the upward  $v_+$  and downward  $v_-$  velocity directions. We, furthermore, consider the energy balance per event and then integrate over the solar surface.

Energy balance per event during the reconnection phase requires:

$$F_{\text{mag}\pm} = F_{\text{rad}\pm} + F_{\text{cond}\pm} + F_{\text{w}\pm} + F_{\text{K}\pm} \quad (10)$$

expressed in terms of fluxes, e.g. in  $\text{erg cm}^{-2} \text{ s}^{-1}$ , where “+” and “-” represent fluxes toward and away from the observer, respectively. The first term on the right hand side of Eq.(10) corresponds to the radiative flux, the second term to the conductive flux along the magnetic field lines, the third to the wave energy flux. The third term, although probably important, will be omitted from the following discussion, since the precise modes and amplitudes of the waves are not known. The last term of Eq.(10) is the sum of three terms, i.e.,

$$F_{\text{K}\pm} = F_{\text{kin}\pm} + F_{\text{enth}\pm} \pm F_{\text{g}\pm} \quad (11)$$

The first term of the right hand side of Eq.(11) represents the kinetic energy flux,  $F_{\text{kin}\pm} = \frac{1}{2} \rho v_{\pm}^3$ , the second term is the enthalpy flux,  $F_{\text{enth}\pm} = \frac{\gamma}{(\gamma-1)} \rho v_{\pm}$ , and the third term is the gravitational energy flux,  $F_{\text{g}\pm} = \rho g \frac{L}{2} v_{\pm}$ , where  $\gamma$ , is the ratio of the specific heats and  $g$  is the acceleration due to solar gravity.  $\gamma$  is taken equal to  $\frac{5}{3}$ , although it must be smaller than this value since we are dealing with a partially ionized gas. Assuming that the mean values for the upward and downward parameters are equal and thus that the upward and downward fluxes are equal, then the total flux components per event during the reconnection phase are given by  $F_{i,t} = F_{i,+} + F_{i,-} = 2F_{i,\pm}$ . For the net radiative loss rate per unit volume we use the analytical expression given by Nagai (1980):

$$e_{\text{rad}} = \alpha(T) N_e^2 \chi g(T) \quad (12)$$

given in  $\text{erg cm}^{-3} \text{ s}^{-1}$ , where  $g(T)$  is a semi-empirical function of the temperature,  $\alpha$  is the radiative reduction coefficient and  $\chi$  is the ionization degree (mean values of all parameters are obtained after averaging over the 2D

**Table 1.** Energy fluxes

Flux in erg cm <sup>-2</sup> s <sup>-1</sup>	per event	global
$F_{\text{rad}}$	$2.7 \cdot 10^6$	$3.4 \cdot 10^4$
$F_{\text{cond}}$	0.44	$5.7 \cdot 10^{-3}$
$F_{\text{kin}}$	$3.4 \cdot 10^6$	$4.4 \cdot 10^4$
$F_{\text{enth}}$	$3 \cdot 10^6$	$3.9 \cdot 10^4$
$F_{\text{total}}$	$9.1 \cdot 10^6$	$1.2 \cdot 10^5$

FOV). According to Nagai (1980) for  $T=10^4$  K,  $g(T) \sim 10^{-23}$  erg cm<sup>3</sup> s<sup>-1</sup> and  $\alpha(T) \sim 0.1$ . Using these values we find that the net radiative loss rate,  $e_{\text{rad}}$  is equal to  $2.7 \cdot 10^{-3}$  erg cm<sup>-3</sup> s<sup>-1</sup>. To calculate the total radiative losses the radiative volume  $V = \pi(\frac{l}{2})^2 L$  is required, where  $l$  is the mean width of the mottles and  $L$  their vertical extent. The radiative loss rate due to radiative cooling is then given by:

$$E_{\text{rad,t}} = e_{\text{rad}} V \quad (13)$$

and is of the order of  $2.1 \cdot 10^{22}$  erg s<sup>-1</sup>, while the radiative flux given by:

$$F_{\text{rad,t}} = e_{\text{rad}} L \quad (14)$$

is equal to  $2.7 \cdot 10^6$  erg cm<sup>-2</sup> s<sup>-1</sup>. The second term on the right hand side of Eq. (10) corresponds to the conductive flux along magnetic field lines:

$$F_{\text{cond,t}} = \kappa \frac{dT}{dh} \quad (15)$$

where  $\kappa = 1.1 \cdot 10^{-6} T^{5/2}$  erg s<sup>-1</sup> cm<sup>-1</sup> K<sup>-1</sup> is the Spitzer thermal conductivity and  $\frac{dT}{dh}$  is the absolute value of the temperature gradient. Equating the relation above to  $2(1.1 \cdot 10^{-6} T^{7/2}/L/2)$  then a conductive flux equal to  $0.44$  erg cm<sup>-2</sup> s<sup>-1</sup> is obtained. From this estimate it can be concluded that the conductive flux is very small and can be neglected.

From the other two fluxes, the kinetic energy flux can be deposited as heat, e.g. by forming shocks and then dissipating via viscosity and conduction. Adopting for the duration of the outflow+downflow phase of each

event a time  $t_i$  equal to 150 s, the contribution of all mottles to the global energy flux can be found from the total individual energy flux multiplied by the area of each event  $S_i$ , the lifetime of the event and the birthrate divided by the surface of the Sun  $S_o$ , e.g.

$$F_{\text{global,t}} = \frac{F_{i,t} S_i t_i b}{2S_o} \quad (16)$$

where the factor 1/2 comes from the assumption that only half of them show the signature of reconnection each time. In Table 1 we summarize the contribution of each structure to each energy flux component, as well as the contribution of all events to the global energetics. Half of their sum gives the contribution of mottles to the energy budget of the solar corona (equal amounts go to the energy budget of the chromosphere). This flux is ~20% of the total flux needed to maintain the solar corona. It should be noted that this value is overestimated since a part of the kinetic and enthalpy fluxes is converted into potential energy, while the gas moves upward and only the remaining part is available for maintaining the coronal energy budget. The energy flux  $F_{\text{total,t}}$  has to balance the total magnetic energy content  $F_{\text{mag,t}}$  released at the reconnection site. Equating these two fluxes we can obtain an estimate of the magnetic field which is found to be of the order of 11 G.

Of course, the values of the different parameters, especially those of the axial velocity and of the birthrate may play an important role on the above estimated flux values. In Fig. 3 we give a contour plot of the kinetic energy flux that goes into heat (left) and of the total magnetic energy flux (right) for velocities in the range 20 – 40 km s<sup>-1</sup> and total number of mottles found on the Sun in the range  $5 \cdot 10^4 - 10^6$ . It is obvious that for low velocities and low total number of mottles the contribution of these structures to the total magnetic energy and to the heating (even if we assume that all the kinetic flux goes into heating) of the solar corona is negligible. However, it is very interesting to note that as the velocity and the number of mottles increase the energy fluxes increase, as well as the percentage of the energy flux that goes into heating.

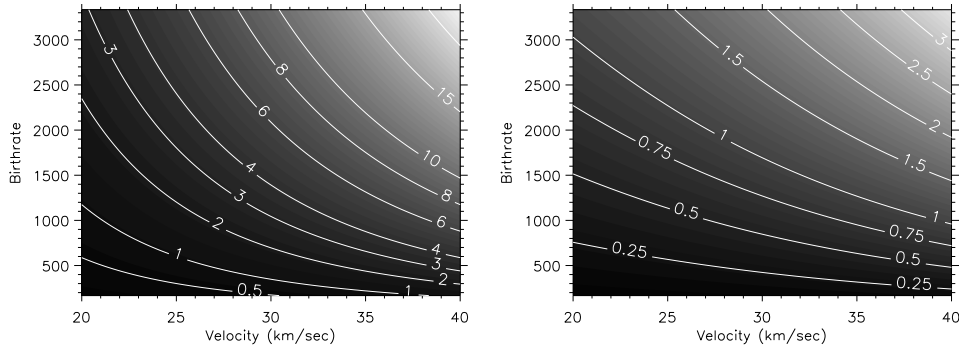


**Fig. 3.** Contour plot of the kinetic flux in units of  $10^4 \text{ erg cm}^{-2} \text{ s}^{-1}$  (left) and of the total magnetic energy flux in units of  $10^5 \text{ erg cm}^{-2} \text{ s}^{-1}$  (right) that goes towards the corona as a function of axial velocity and mottle birthrate

## 5. Conclusions

Our results highlight the importance of two-dimensional observations, like the ones provided by the MSDP spectrograph, for the study of the dynamical behaviour of evolving solar structures. From these observations several physical parameters describing chromospheric dark mottles have been obtained by means of the cloud model. The deduced physical parameters of mottles and their temporal variations have been proved very useful in obtaining, at least, order of magnitude estimates of the different processes that contribute to the mass balance and heating of the solar corona and to derive estimates of the energy released by magnetic reconnection.

We have found that mottles supply material to the solar corona much in excess of that needed to compensate for coronal mass losses in the solar wind. Thus mottles could be the physical means by which is established the overall mass balance in the solar atmosphere. Mottles, as well as spicules, transport also energy high up in the upper chromosphere and corona. Using some typical values for the velocity and their total number then the sum of the bulk kinetic energy, of the enthalpy energy and of the radiation losses could account for at most  $\sim 20\%$  of the total coronal energy losses. However, from all these energy fluxes only part of the kinetic energy is deposited as heat. If this is the case then mottles by themselves do not

transfer enough energy to heat the corona. On the other hand, it is possible that the total energy released that goes into heat may be substantially larger from the kinetic energy, because of the reconnection that can release a large fraction of its energy as MHD waves, the role of which, however, it is not easy to be treated quantitatively. In this context further work is needed in order to better establish the role of mottles in the heating of the solar atmosphere.

*Acknowledgements.* The authors thank the meeting organizers for providing financial support.

## References

- Alissandrakis, C. E., Tsiropoula, G., & Mein, P. 1990, *A&A* 230, 200.
- Beckers, J.M. 1964, Ph.D. Thesis, Utrecht.
- Mein, P. 1991, *A&A* 248, 669
- Mein, P. 2002, *A&A* 381, 271
- Nagai, F. 1980, *Solar Phys.*, 68, 351
- Tsiropoula, G., Alissandrakis, C.E., & Schmieder, B. 1994, *A&A* 290, 285
- Tsiropoula, G., & Schmieder, B. 1997, *A&A* 324, 1183
- Tsiropoula, G., & Tziotziou, K. 2004, *A&A* 424, 279
- Tziotziou, K., Tsiropoula, G., & Mein, P. 2003, *A&A*, 402, 361
- Ulmschneider, P. 1971, *A&A* 12, 297
- Wilhelm, K. 2000, *A&A* 360, 351